 DOI: 10.1002/masy.200951220

In-Situ Formation of Silver Nanoparticles in PEI

S. Cotts,[1] *J. Compton,*[1] *D. Kranbuehl,**[1] *E. Espuche,*[2] *L. David,*[2] *G. Boiteux*[2]

Summary: Nanocomposites consisting of spherical particles of Ag were prepared using a single step in situ method whereby Ag is introduced into the dissolved polymer via dissolution as the organometallic complex Ag TFA in the same solvent as the polymer. The kinetic rate of formation of the particles is determined using WAXS and SAXS measurements. Nanoparticle formation is found to depend on reducing the solvent/polymer ratio, which leads to de-solvating the metal complex. This destabilizes the metal precursor complex, causing it to degrade and the metal particles to phase separate by a thermodynamic driving force. The size of the nanoparticles varies with the cure temperature and the conditions affecting molecular mobility.

Keywords: organometallic complex; silver nanoparticles

Introduction

Nanocomposites have been the subject of extensive research due to their unique abilities to enhance the properties of bulk materials.[1–15] Alumina-silicate-polymer hybrids have been the focus of much of this research because of the high length-thickness ratio of lamellar sheets and their role in improving gas barrier properties.[9,11,13,14,16] However, the complex and varied dimensions of each layer makes it difficult to develop a fundamental understanding of the role of bulk-particle interactions.

A hybrid material consisting of spherical particles of different composition that can be homogeneously incorporated into the matrix is ideal for understanding the fundamental effects of nanoparticles on nanoparticle-polymer properties. A single-step method for incorporating metal into polymer substrates has been established whereby the metal is introduced into the dissolved polymer via dissolution as an organometallic complex in the same solvent as the polymer and subsequently mixed. [2,3,5,7,17–21] This solution is then cast and thermally treated thereby forming nanoparticles. Previous research has shown, for example, a marked improvement in the gas-barrier properties in films while not greatly affecting any other mechanical properties.[7,18] For example, incorporating nanoparticles from silver complexes in polyimides can result in electrically conductive and reflective surfaces.

The work discussed herein focuses on studying the influences, kinetics, and control of Ag particle growth in the well known substrate polyetherimide while also observing some final bulk properties of the materials. Previous studies have shown the effects of varying cure conditions on material properties, but have not explored the kinetics and mechanism for particle formation. The effect of cure temperature was the first variable to be studied on each of the three systems because it is believed that curing conditions can alter the final properties of similar systems. During these experiments, it became evident that solvent loss played a large role in particle formation, perhaps more so than thermal degradation of the metal precursor complex. Thus, the focus of the experiments changed to controlling both temperature and solvent loss to attempt to demonstrate the effect of the solvent/polymer ratio on the kinetics of nanoparticle formation. In order to demonstrate the effect solvent loss plays, correlation of the start of particle formation, the kinetic curve, and the final particle

[1] College of William and Mary, Williamsburg, VA, USA
Fax: 757-221-2715; E-mail: dekran@wm.edu
[2] University of Lyon, France

size as measured by the change in the solvent polymer weight ratio became an important goal for these experiments

Experimental Part

Film Preparation

Poly(Bisphenol Poly(Bisphenol A-*co*-4-nitrophthalic anhydride-*co*-1,3-phenylenediamine) (PEI) and silver trifluoroacetate (TFA) were purchased from Aldrich Chemical and used as received. PEI was dissolved using anhydrous dimethylacetamide (DMAc) which was purchased from Aldrich chemical. The mixture dissolved slowly at room temperature, so the solution was placed on slight heat (~40 °C) to increase dissolution rate. Once dissolved, the solution was allowed to continue stirring while the solution cooled back to room temperature. In the meantime, a silver TFA was dissolved in DMAc also and allowed to stir for ~2 hr to ensure complete dissolution. Once both the polymer and metal precursor have been dissolved, the metal precursor solution is added to the polymer solution which is then allowed to continue stirring for ~2 hr more.

Films were cast on soda-lime glass plates using a doctor blade set to 0.610 mm. These films were then allowed to dry in a plexiglass drybox with approximately 2% humidity overnight to remove the majority of the solvent until tact-free. These films were then cured in a Blue M Electric Forced Air Oven, a Thermolyne 47900 Furnace, or a Precision Vacuum Oven Model 19. Films were cured at different temperatures for different amounts of time- at 140° for 48 hours, at 140° under vacuum for 36 hours, followed by 2 hours at 240°, at 190° for 4 hours and at 240° for 4 hours.

Characterization

Characterization techniques include thermogravimetric analysis (TGA), differential scanning calorimetry (DSC), x-ray diffraction (XRD), small angle x-ray scattering (SAXS), and transmission electronic microscopy (TEM). For DSC experiments, the samples were ramped at 10 °C/min to 240 °C, held isothermally for 30 min, cooled at 1 °C/min to 160 °C, and cycled two more times to verify that all of the solvent had been removed and that the T_g was no longer shifting. The TGA procedure was to ramp the sample to 240 °C at 10 °C/min and then held isothermally for 90 min to ensure all of the solvent had been removed. The growth of nanoparticles was followed by SAXS experiments performed at the European Synchrotron Radiation facility in Grenoble, France and by XRD performed on a Bruker System with 3-circle goniometer. For SAXS, a Ropper Scientific CCD camera was used and scattering diagrams are obtained after radial averages around the image center. The data were collected over a range of exposure times, at incident photon energy of 16 keV, and using silver behenate as a q-range calibration standard. Dielectric measurements were made of neat films and silver films during cure in Lyon, France. TEMS were also performed in Lyon on cross sections of cured films.

Results and Discussion

Thermogravimetric experiments were run to measure and record the evolution of solvent loss in the polymer films during and after cure. Complete removal of solvent is necessary to determine a true T_g. After inspection of some TGA results, solvent loss appeared to parallel nanoparticle formation. Previous studies suggested that all but a negligible amount of solvent is removed from films by drying alone; however, reduction in the films' weights after curing was too great to attribute to the loss of the complex alone. After extensive drying, some solvent remains solvated to the precursor metal complex. In neat PEI films, holding at 240 °C results in a loss of 10% of the mass due to solvent evaporation, and in Ag films, the mass lost is 14%, indicating that the silver precursor binds extra solvent.

DSC measurements confirmed the existence of residual solvent in dried films. DSC

runs were repeated to remove excess solvent, and as the amount of solvent is decreased, the sample's T_g increases towards the true value. The presence of silver nanoparticles formed at 240 °C increased the T_g from 215.2° (the T_g of neat PEI) to 216.5°. This increase suggests that silver has a small effect on hindering polymer chain mobility. Nanoparticles formed at 140° had no significant effect on T_g.

Previous work has shown that silver forms crystalline nanoparticles that can be detected by XRD. Neat PEI is run first to establish the diffraction pattern for the polymer alone. One large broad peak was shown at $2\theta = 18°$ and a smaller very broad peak at $2\theta = 7°$ for the neat amorphous PEI film. The silver complex XRD spectra show the onset of metallic silver nanoparticle formation at 140 °C at $2\theta = 48.5°$. Further post curing at 240 °C shows a much larger and sharper peak at each of the expected metallic silver angles. Figure 1 shows the spectra of neat PEI and thermally cured silver films. The Debye-Scherrer equation predicts the XRD peak will become larger and sharper as the metal nanoparticles increase in size. This coalescing of the Ag atoms to form more ordered and larger particles is occurring for the Ag-PEI system with loss of additional solvent as seen in Figure 1.

SAXS experiments were run on these samples isothermally cured at 140 °C, 190 °C and 240 °C for more precise measurement of the nanoparticle size and separation. Quantifying the size of the particles was accomplished using the Beaucage model which fits the shape of the low angle scattering in both the Guinier and Porod regions to calculate a more accurate particle size and distribution. Each material is cured at various temperatures, removing samples from the oven at various times to be run on the beamline. The sample is then inundated with x-rays in the beamline until an appropriate amount of scattering is collected. Figure 2 shows the scattering for Ag-PEI films that have been air dried, cured at 140°, vacuum cured at 140° and post cured at 240°. R_g values calculated from scattering data indicated that the samples cured at higher temperatures have larger particles. The sizes of silver nanoparticles from different curing temperatures are shown in Table 1. We propose that the increased mobility of the polymer chains at higher temperatures, particularly above T_g, increases the ability of these metal atoms to form with particles further away. At lower

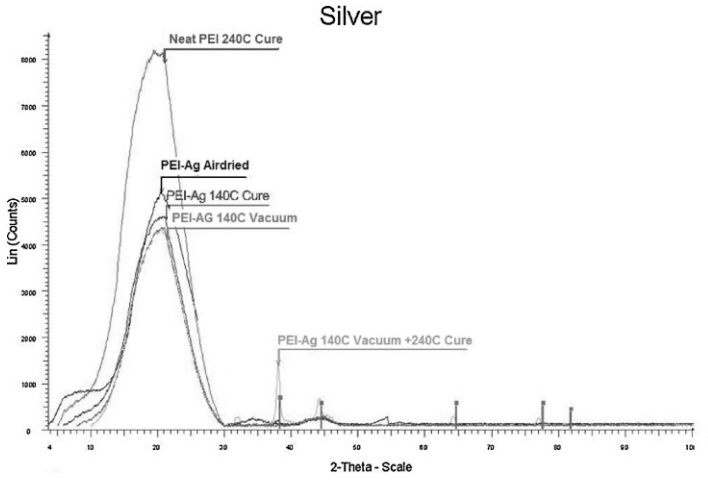

Figure 1.
XRD spectra for neat PEI thermally cured Ag films.

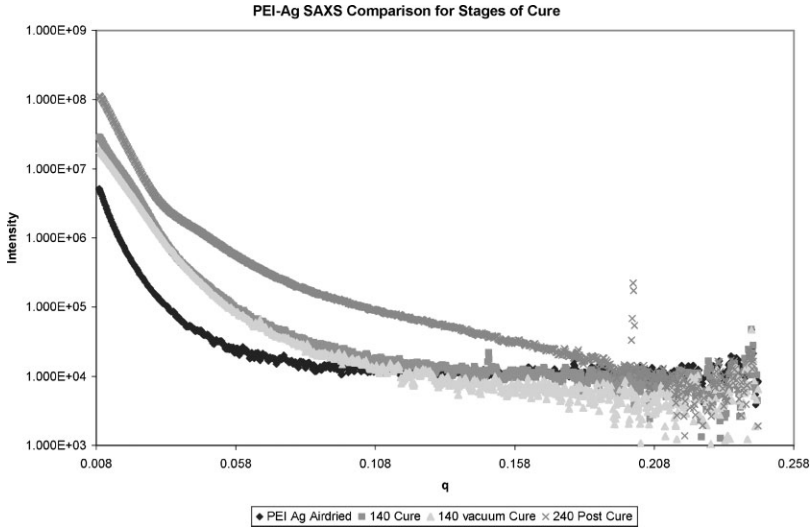

Figure 2.
SAXS scattering intensity vs angle q for PEI-Ag films.

temperatures, particularly below T_g where the polymer chains hinder the movement of the complex, smaller Ag nanoparticles are formed. This phenomenon is demonstrated in Table 1 where the R_g values of the Ag systems increase with their respective cure temperature. Based on the SAXS results, the PEI-Ag system takes about 15 minutes until the particles are completely formed.

Based on TGA, SAXS and WAXS data, particle formation can be correlated with solvent loss. The formation of particles, as seen in SAXS and WAXS, is plotted with the solvent content of the system (as determined by TGA) as a function of time for 240 °C (Figure 3) and 140 °C (Figure 4). At the onset of silver particle formation in the 240° system, the solvent content is about 6%, and at around 3%, particle formation stops due to the decreased mobility in the glassy state. The relationship is different in the 140° system- the onset of silver particle formation occurs at 14.5% solvent, and is stopped when solvent content decreases to 10% due to decreased mobility. Nanoparticle formation is driven by the thermodynamic instability of the precursor complex as the concentration increases due to the decrease in the ratio of solvent to polymer. The nanoparticle formation process is not a temperature dependent kinetic degradation of the complex, but rather a process involving the rate of solvent removal to a value of the solvent/polymer ratio where phase separation and complex disintegration occurs. At higher temperatures, the solubility of the precursor is great, and a smaller solvent/polymer ratio must be achieved before the dissolved complex becomes unstable and decompose.

Dielectric measurements show at what points during cure solvent is lost and particles are formed. Dielectrically monitoring the cure of a neat PEI film at 140 °C shows a sharp peak at the beginning that drops of as the film is held at that temperature, corresponding to solvent loss. The same procedure applied to a silver-PEI film shows a similar sharp peak due to solvent loss, followed by a broad peak in the next 20 minutes, corresponding to the

Table 1.
Rg Values of Silver Nanoparicles

140	140v	140v + 240	190	240
11.2	15.2	15.3	18.8 (20.2)	26.1 (23.2)

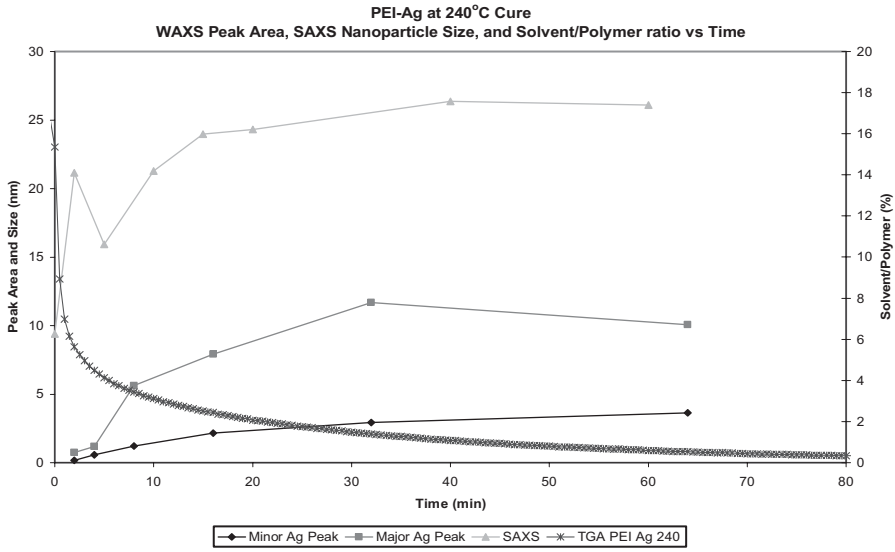

Figure 3.
Nanoparticle formation as measured by SAXS and WAXS, and solvent:polymer ratio as measured by TGA, as a function of time, at 240 °C.

formation of silver nanoparticles. (Figure 5) For the Ag-PEI films, the value of the permittivity is much larger due to the charge polarization on the surface of the conductive Ag nanoparticles embedded in the nonconductive PEI.

In TEM images of 240° cured silver films, it is clear that the particles on the

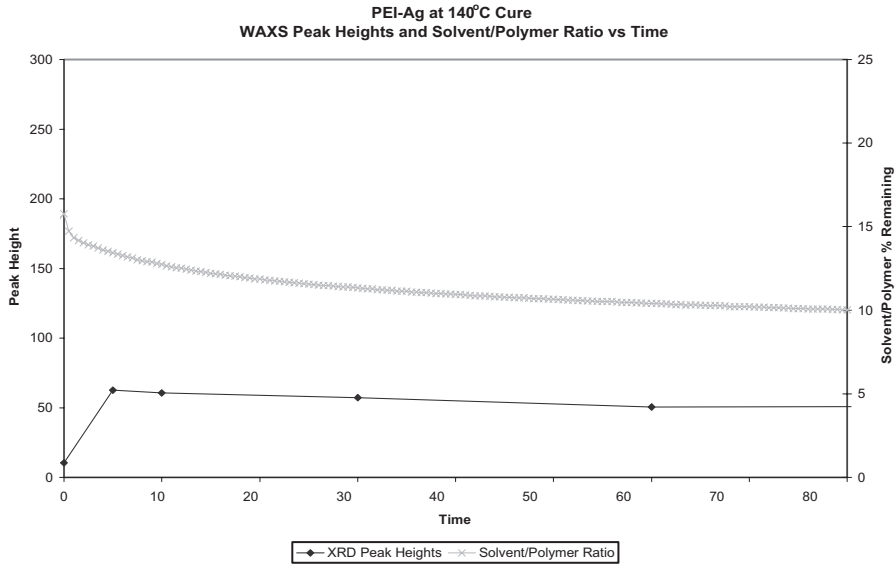

Figure 4.
Nanoparticle formation as measured by SAXS and WAXS, and solvent:polymer ratio as measured by TGA, as a function of time, at 140 °C.

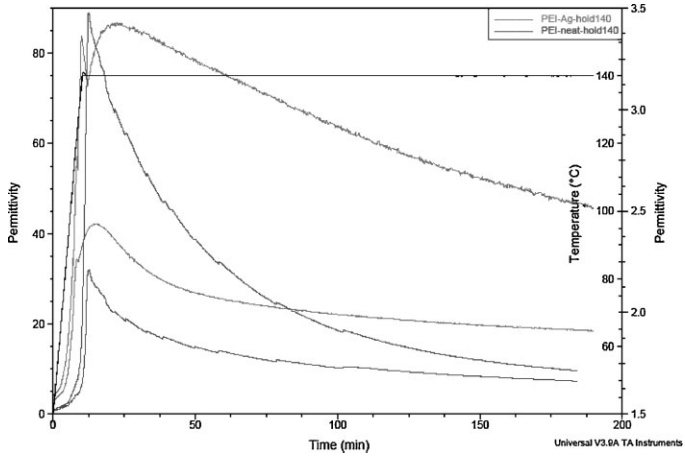

Figure 5.
Permitivity of neat PEI and Ag films during 140 °C cure.

surface of the film are much larger than those in the interior, which is consistent with the observations that particle formation is driven by solvent loss. Figure 6 shows a cross section of a silver film cured at 240°, including the surface; Figure 7 shows a more magnified area of the interior of the film. Interior particles are around 25–35 nm in diameter, while the exterior particles are 510 nm.

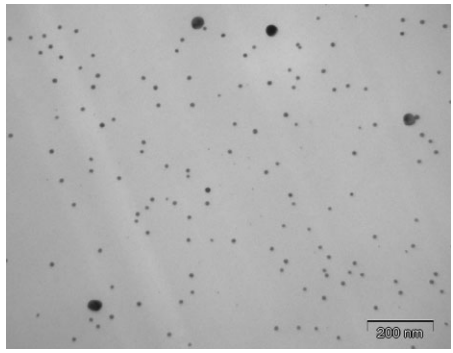

Figure 7.
TEM of Ag film cured at 240 °C.

Conclusion

Silver nanoparticles were formed in situ in PEI. Nanoparticle formation is based on reducing the solvent/polymer ratio, desolvating the Ag-TFA complex. This destabilizes the precursor complex, causing it to degrade and the silver particles to phase separate by a thermodynamic driving force. The size of the particles is dependent on the cure temperature and the conditions affecting molecular mobility.

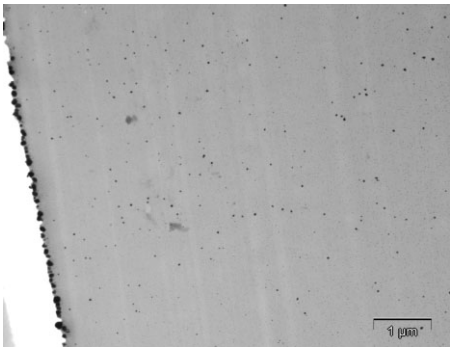

Figure 6.
TEM of Ag film cured at 240 °C.

[1] Z. Ahmad, J. E. Mark, Polyimide-ceramic hybrid composites by the sol-gel route. *Chemistry of Materials* **2001**, *13*, 3320–3330.

[2] L.-J. Bian, X.-F. Qian, J. Yin, Z.-K. Zhu, Q.-H. Lu, Eu^{3+} complex/polyimide nanocomposites: improvement in mechanical and thermal properties. *Journal of Applied Polymer Science* **2002**, *86*, 2707–2712.

[3] P.-C. Chiang, W.-T. Whang, M.-H. Tsai, S.-C. Wu, Physical and mechanical properties of polyimide/titania hybrid films. *Thin Solid Films* **2004**, *447–448*, 359–364.

[4] B. J. Chisholm, R. B. Moore, G. Barber, F. Khouri, A. Hampstead, M. Larsen, E. Olson, J. Kelley, G. Balch, J. Caraher, Nanocomposites Derived from Sulfonated Poly(butylene terephthalate). *Macromolecules* **2002**, *35*(14), 5508–5516.

[5] L. M. Davis, J. M. Compton, D. E. Kranbuehl, D. W. Thompson, R. E. Southward, Reflective and Electrically Conductive Palladium Surface-Metallized Polyimide Nanocomposite Membranes. *Journal of Applied Polymer Science* **2006**, *102*, 2708–2716.

[6] S. Despond, E. Espuche, N. Cartier, A. Domard, Barrier Properties of Paper-Chitosan and Paper-Chitosan-Carnauba Wax Films. *Journal of Applied Polymer Science* **2005**, *98*, 704–710.

[7] E. Espuche, L. David, J. L. Afeld, J. M. Compton, D. E. Kranbuehl, Characterization and Properties of Hybrid Nanoparticle ''inactive and active'' Metal Polymer Films. *Macromolecular Symposia* **2005**, *228*, 155–165.

[8] G. A. Gaddy, G. A. Miner, D. M. Stoakley, E. P. Locke, R. L. Moore, J. Schultz, D. Creyts, M. Knotts, Optical and Mechanical Properties of Photoassisted, Self-assembled Nanoparticle Films. *Materials Research Society Symposium Proceedings* **2004**, *797*, W5.17.1–W5.17.6.

[9] O. Gain, E. Espuche, E. Pollet, M. Alexandre, P. H. Dubois, Gas Barrier Properties of Poly(ε-caprolactone)/Clay Nanocomposites: Influence of the Morphology and Polymer/Clay Interactions. *Journal of Polymer Science: Part B: Polymer Physics* **2005**, *43*, 205–214.

[10] P. J. F. Harris, Carbon nanotube composites. *International Materials Reviews* **2004**, *49*, (1). 31–43.

[11] E. Jacquelot, E. Espuche, J.-F. Gérard, J. Duchet, P. Mazabraud, Morphology and Gas Barrier Properties of Polyethylene-Based Nanocomposites. *Journal of Polymer Science: Part B: Polymer Physics* **2006**, *44*, 431–440.

[12] C. Park, Z. Ounaies, K. A. Watson, R. E. Crooks, J. Smith, Jr., S. E. Lowther, J. W. Connell, E. J. Siochi, J. S. Harrison, T. L. St. Clair, Dispersion of single wall carbon nanotubes by in situ polymerization under sonication. *Chemical Physics Letters* **2002**, *364*, 303–308.

[13] E. Picard, H. Gauthier, J.-F. Gérard, E. Espuche, Influence of the intercalated cations on the surface energy of montmorillonites: Consequences for the morphology and gas barrier properties of polyethylene/montmorillonites nanocomposites. *Journal of Colloid and Interface Science* **2007**, *307*, 364–376.

[14] E. Picard, A. Vermogen, J.-F. Gérard, E. Espuche, Barrier properties of nylon 6-montmorillonite nanocomposite membranes prepared by melt blending: Influence of the clay content and dispersion state Consequences on modelling. *Journal of Membrane Science* **2007**, *292*, 133–144.

[15] J. G. Smith, Jr., J. W. Connell, D. M. Delozier, P. T. Lillehei, K. A. Watson, Y. Lin, B. Zhou, Y.-P. Sun, Space durable polymer/carbon nanotube films for electrostatic charge mitigation. *Polymer* **2004**, *45*, 825–836.

[16] Y. Fukushima, S. Inagaki, Synthesis of an intercalated compound of montmorillonite and 6-polyamide. *Journal of Inclusion Phenomena and Macrocyclic Chemistry* **1987**, *5*(4), 473–482.

[17] S. Clémenson, P. Alcouffe, L. David, E. Espuche, Structure and morphology of membranes prepared from polyvinyl alcohol and silver nitrate: influence of the annealing treatment and of the film thickness. *Desalination* **2006**, *200*, 437–439.

[18] J. Compton, D. Thompson, D. Kranbuehl, S. Ohl, O. Gain, L. David, E. Espuche, Hybrid films of polyimide containing in situ generated silver or palladium nanoparticles: Effect of the particle precursor and of the processing conditions on the mophology and the gas permeability. *Polymer* **2006**, *47*, 5303–5313.

[19] E. Espuche, L. David, C. Rochas, J. L. Afeld, J. M. Compton, D. W. Thompson, D. S. Thompson, D. E. Kranbuehl, In situ generation of nanoparticulate lanthanum (III) oxide. *Polymer* **2005**, *46*, 6657–6665.

[20] A. K. St. Clair, V. C. Carver, L. T. Taylor, T. A. Furtsch, Electrically Conductive Polyimide Films Containing Palladium Coordination Complexes. *Journal of the American Chemical Society* **1980**, *102*, 876–878.

[21] D. S. Thompson, D. W. Thompson, R. E. Southward, Oxo-Metal-Polyimide Nanocomposites. 2. Enhancement of Thermal, Mechanical, and Chemical Properties in Solubable hexafluoroisopropylidine-Based Polyimides via the in Situ Formation of Oxo-Lanthanide(III)-Polyimide Nanocomposites. *Chemistry of Materials* **2002**, *14*(1), 30–37.

[22] J. D. Warner, M. Pevzner, C. J. Dean, D. E. Kranbuehl, J. L. Scott, S. T. Broadwater, D. W. Thompson, R. E. Southward, Synthesis of hexafluoroisopropylidene-containing polyimide silver nanocomposite films evolving specularly reflective metal surfaces. *Journal of Materials Chemistry* **2003**, *13*, 1847–1852.

[23] L. M. Davis, D. S. Thompson, D. W. Thompson, R. E. Southward, Silver-polyimide nanocomposite films: A single-stage thermally-induced metallization of aromatic fluorinated polyimides yielding highly reflective films., In: *Polyimides and Other High*

Temperature Polymers, K. L. Mittal, Ed., VSP: **2007**, *Vol. 4*, pp 261–286.
[24] R. E. Southward, D. S. Thompson, T. A. Thornton, D. W. Thompson, A. K. St. Clair, Enhancement of Dimensional Stability in Soluble Fluorinated Polyimides via the in Situ Formation of Lanthanum(III)-Oxo-Polyimide Nanocomposites. *Chemistry of Materials* **1998**, *10*(2), 486–494.
[25] L. M. Daniel, R. L. Frost, H. Y. Zhu, Synthesis and characterisation of clay-supported titania photocatalysts. *Journal of Colloid and Interface Science* **2007**, *316*(1), 72–79.
[26] G. Beaucage, D. W. Schaefer, Structural studies of complex systems using small-angle scattering: a unified Guinier/power-law approach. *Journal of Non-crystalline Solids* **1994**, *172-174*(2), 797–805.

